Essential function of protein 4.1G in targeting of MPP6 into Schmidt-Lanterman incisures in myelinated nerves

Nobuo Terada, [1,2] Yurika Saitoh, [1] Nobuhiko Ohno, [1] Masayuki Komada, [3]

Sei Saitoh, [1] Elior Peles, [4] and Shinichi Ohno[1]

1. Department of Anatomy & Molecular Histology, Interdisciplinary Graduate School of Medicine and Engineering, University of Yamanashi, Chuo-city, Yamanashi, Japan.
2. Department of Occupational Therapy, School of Health Sciences, Shinshu University School of Medicine, Matsumoto-city, Nagano, Japan.
4. Department of Biological Sciences, Tokyo Institute of Technology, Yokohama-city, Kanagawa, Japan.
5. Department of Molecular Cell Biology, Weizmann institute of Science, Rehovot, Israel.

Running title: 4.1G Targets MPP6 into Schmidt-Lanterman incisures.

Corresponding author: Nobuo Terada, M.D., Ph.D.
Department of Occupational Therapy,
School of Health Sciences,
Shinshu University School of Medicine,
3-1-1 Asahi, Matsumoto-city,
Nagano 390-8621, Japan
Tel and Fax: +81-263-37-2412
E-mail: nobuot@shinshu-u.ac.jp

ABSTRACT

Protein 4.1G is a membrane skeletal protein found in specific subcellular structures in myelinated Schwann cells and seminiferous tubules. Here we show that in the mouse sciatic nerve, protein 4.1G colocalized at Schmidt-Lanterman incisures (SLI) and the paranodes with a member of the Membrane-Associated Guanylate Kinase (MAGUK) family, Membrane Protein Palmitoylated 6 (MPP6). Co-immunoprecipitation experiments revealed that MPP6 was interacting with protein 4.1G. In contrast to wild type nerves, in 4.1G-knockout mice, MPP6 was largely found in the cytoplasm near Schwann cell nuclei, indicating an abnormal protein transport. Although the SLIs remained in the 4.1G-knockout sciatic nerves, as confirmed by E-cadherin immunostaining, their shape was altered in aged 4.1G-knockout compared to the wild-type nerves. In the seminiferous tubules, MPP6 was localized similar to protein 4.1G along cell membranes of the spermatogonium and early spermatocytes. However, in contrast to myelinated peripheral nerves, the specific localization of MPP6 in the seminiferous tubules was unaltered in the absence of protein 4.1G. These results indicate that 4.1G has a specific role in the targeting of MPP6 to the SLI and the assembly of these subcellular structures.

INTRODUCTION

Protein 4.1G (4.1G) is a member of the 4.1 family (27, 46), which are membrane skeletal proteins that link various components to the spectrin-actin network (10). We have previously reported that 4.1G is present in rodent Schwann cells (7, 24) and mouse seminiferous tubules (40, 41). In peripheral nerves, 4.1G is found at the Schmidt-Lanterman incisures (SLI) and the paranodal loops of myelinated Schwann cells (24). The SLI are funnel-shaped interruptions within the myelin sheath of nerve fibers. They contain high concentration of actin and spectrin (35, 42), which forms a membrane skeleton that might contribute the elasticity and stability of these structures.

Membrane-associated Guanylate kinase (MAGUK) family proteins contain PDZ [PSD (postsynaptic density)-95 / Dlg (Drosophila disks large) / ZO (zonula occludens)-1], GUK (guanylate kinase) and SH3 (src-homology-3) domains, and they localize to specific domains at the plasma membranes (9, 11). In epithelial cells for example, some MAGUKs, such as Dlg and ZO-1, are required for the formation of adherens and tight junctions, respectively. In addition to their function as membrane scaffolds (16, 21), several MAGUKs also control intracellular protein transport through their ability to bind motor proteins (45, 49). Interestingly, some MAGUKs contain specific domains that interact with 4.1 proteins (14, 17, 18). In the current study we report the identification of Membrane Protein Palmitoylated 6 (MPP6) (also known as PALS2, VAM1 and p55T; http://www.genenames.org/), as a novel

MAGUK molecule that interact with 4.1G in peripheral nerves. We further demonstrate that the interaction between 4.1G and MPP6 is essential for the targeting of the latter into SLI.

MATERIALS AND METHODS

Animals and anesthesia. All animal experiments were performed in accordance with the guidelines of the Animal Care and Use Committee of the University of Yamanashi. Production of the $4.1G^{-/-}$ (37) and $4.1B^{-/-}$ (23) mice was previously described. Adult (10 month old) wild type, $4.1G^{-/-}$, $4.1B^{-/-}$, and double-knockout $4.1G^{-/-}B^{-/-}$ mice (n=6 mice for each genotype) were anesthetized with pentobarbital and processed for the following preparation procedures.

In vivo cryotechnique (IVCT) for living mouse sciatic nerves and subsequent freeze-substitution fixation (FS). IVCT was performed on the exposed sciatic nerves of the anesthetized mice by directly pouring 50 ml liquid isopentane-propane cryogen (-193^{o}C) cooled in liquid nitrogen, as previously described (38). The frozen nerves were removed with a dental electric drill in liquid nitrogen, and processed for routine FS in acetone containing 2% paraformaldehyde at -80^{o}C for 24 h and then at -30^{o}C, -10^{o}C, 4^{o}C and RT for 2 h each, as described (41). They were washed in pure acetone and xylene, and embedded in paraffin.

Perfusion fixation followed by teasing for sciatic nerves or sucrose embedding for testes. To obtain perfusion-fixed sciatic nerves or testes, anesthetized mice were perfused with 2% paraformaldehyde in 0.1 M phosphate buffer (PB, pH 7.4) via the heart. The sciatic nerves or testes were then removed and immersed in the same fixative at 4°C for 2 h. To produce teased nerve fibers, the fixed sciatic nerves were separated with fine needles under a stereomicroscope, and frozen with isopentane precooled in dry ice. The frozen nerves were then thawed in phosphate buffered saline (PBS, pH 7.4) at room temperature (RT), frozen-thawed again, and then used for the immunostaining. For some teased sciatic nerves, the frozen-thawed treatment was not performed, and heights of the SLI-circular truncated cones with immunostaining and phalloidin staining, described in the next section, were measured. Testes were rinsed in PBS, immersed in 30% sucrose/5% glycerol in PB at 4°C overnight, embedded in optimum cutting temperature (OCT) compound (Tissue-Tek, Sakura Finetechnical, Tokyo, Japan), and frozen with isopentane precooled in dry ice.

Immunostaining and phalloidin staining for light microscopic observation. For paraffin-embedded IVCT-FS sciatic nerves, 4 μm-thickness sections were cut, routinely de-paraffinized with xylene, and infiltrated in a graded series of ethanol and PBS. For sucrose-embedded frozen testis tissues, 6-8 μm-thickness cryosections were cut in a cryostat machine, and infiltrated into PBS. Some deparaffinized sections were stained with

hematoxylin-eosin (HE) for pure morphology at the light microscopic level. For common immunostaining, sections were pre-treated with hydrogen peroxide and normal goat serum, followed by rabbit polyclonal anti-MPP6 antibody (Ab) (Sigma, St Louis, MO, USA), anti-4.1G Ab (ProteinExpress, Kisarazu, Ibaraki, Japan) or rat monoclonal anti-E-cadherin Ab (Takara BioInc., Ohtsu, Shiga, Japan) at 4^{o}C overnight. They were treated with biotinylated anti-rabbit or anti-rat IgG Abs (Vector, Burlingame, CA, USA) at RT for 1 h, then a horseradish peroxidase-labeled avidin-biotin complex (ThermoSci., Rockford, IL, USA) at RT for 1 h, and visualized with a metal-enhanced diaminobenzidine (DAB) method (ThermoSci.). Finally, they were incubated in 0.04% osmium tetroxide solution for 30-60 sec, and observed under a light microscope. Staining with only the secondary anti-rabbit or rat IgG antibodies was used as controls.

For double-immunofluorescence staining for MPP6 and E-cadherin, the teased sciatic nerves were treated with PBS containing 0.1% Triton X-100 (PBS-T) at RT for 2 h, and incubated with both rabbit polyclonal anti-MPP6 (Sigma) and rat monoclonal anti-E-cadherin (Takara) Abs at the same time in PBS-T at 4^{o}C overnight. Then, they were treated with Alexa Fluor 488-conjugated anti-rabbit IgG and Alexa Fluor 594-conjugated anti-rat IgG Abs (Invitrogen, Carlsbad, CA, USA) at RT for 1 h.

For fluorescence double-staining for E-cadherin and filamentous actin, teased sciatic nerves were incubated with Alexa Fluor 488-conjugated phalloidin (Invitrogen) and rat

anti-E-cadherin Ab at the same time in PBS-T at 4^{o}C overnight. Then, they were treated with Alexa Fluor 594-conjugated anti-rat IgG Ab (Invitrogen) at RT for 1 h.

They were observed under a fluorescence microscope (FM) or confocal laser-scanning microscope (CLSM: FV1000; Olympus, Tokyo, Japan). Measurement of SLI circular truncated cone height with the E-cadherin immunostaining and the phalloidin staining was performed for six hundred SLIs in three 4.1G$^{+/+}$ or 4.1G$^{-/-}$ mice each. The P-value was performed with Student's t-test after evaluating their normal distribution.

Pre-embedding immunoelectron microscopy. Conventional pre-embedding immunoelectron microscopy was performed for the mouse testes as reported before (36). Briefly, anesthetized mice were perfused via their hearts with 2% paraformaldehyde in PB, and cryostat sections were produced and immunostained in the same way as for the sucrose-embedded testis cryosections described in the previous section. After immunostaining, sections were fixed again with 0.25% glutaraldehyde in PB for 10 min, and visualized by the DAB method. Then, they were additionally treated with 1% OsO_4 in PB for 20 min, dehydrated with a graded series of ethanol and embedded in epoxy resin by the inverted gelatin capsule method. Ultrathin sections of 70 nm-thickness were cut on an ultramicrotome and collected on copper grids. They were stained only with uranyl acetate, and observed in an electron microscope (H-7500; Hitachi, Tokyo, Japan) at an accelerating

voltage of 75 kV.

Immunoblotting and immunoprecipitation analyses. For immunoblotting, sciatic nerves of the $4.1G^{+/+}$ or $4.1G^{-/-}$ mice were immersed in Laemmli sample buffer, and the lysate protein concentration was adjusted by measurement with a protein assay kit (ThermoSci.). Following SDS-PAGE and Western blotting was performed with an anti-MPP6 Ab. The blots were visualized using a chemiluminescent system (ThermoSci.).

Immunoprecipitation analysis was performed for the adult $4.1G^{+/+}$ mouse sciatic nerves. To examine the 4.1G-MPP6 `interactions, tissue lysates were obtained from the sciatic nerve supernatant by homogenization with a TENT buffer (20 mM Tris pH 7.4, 1 mM EDTA, 50 mM NaCl, 1% Triton X-100) containing a protease inhibitor cocktail (Sigma) and centrifugation at 10,000 g at 4^{o}C for 30 min. The lysates were treated with protein G-Sepharose (GE Healthcare, Piscataway, NJ, USA) at 4^{o}C for 2 h to remove non-specific reactive proteins to protein G such as mouse IgGs. They were then incubated with a rabbit anti-MPP6 Ab that was the same for the immunohistochemistry, rabbit anti-4.1G Ab (Bethyl Lab. Inc., Montgomery, TX, USA), or rabbit IgG (Thermo Fisher Scientific, Cheshire, UK) at 4^{o}C for 3 h. Then, immunoprecipitated molecular complexes were separated using protein G-Sepharose at 4^{o}C for 2 h. All proteins were eluted from the Sepharose beads by boiling in Laemmli sample buffer, and then subjected to SDS-PAGE and Western blotting analyses with

the anti-4.1G Ab (ProteinExpress) or anti-MPP6 Ab.

RESULTS

Immunolocalization of MPP6 in sciatic nerves of wild type and 4.1G$^{-/-}$ sciatic nerve.

In IVCT-FS samples of adult sciatic nerves, which preserve soluble proteins well in tissue sections (30), MPP6 immunoreactivity was detected in regions of non-compact myelin, including the SLI and the paranodes (Fig. 1A). Such localization is reminiscent of the one we previously reported for 4.1G (24). Given that 4.1-family proteins could bind to MPPs (22), we examined the expression of MPP6 in sciatic nerves isolated from mice lacking protein 4.1G (Fig. 1B). MPP6 was not detected in the SLI of 4.1G$^{-/-}$ nerve fibers, and it was weakly observed in cytoplasm around nuclei of Schwann cells (Fig. 1B). However, similar to wild type nerves, MPP6 immunoreactivity was still detected in paranodes of 4.1G$^{-/-}$ fibers (the bottom lane in Fig. 1B).

Since the localization and intensity of the MPP6 immunostaining was different in the 4.1G$^{-/-}$ mice, we compared the total amounts of this protein between wild type and 4.1G$^{-/-}$ nerves by immunoblotting (Fig. 1C). As depicted in Fig. 1C, the amount of MPP6 in the 4.1G$^{-/-}$ mice was markedly reduced compared to wild type animals.

Molecular interaction of MPP6 with 4.1G.

Using serial sections of sciatic nerves labeled for protein 4.1G and MPP6, we showed that both proteins co-localized at the SLIs (Fig. 2A). We next examined whether MPP6 and protein 4.1G interact in the sciatic nerve. Nerve lysates were prepared and subjected to immunoprecipitation with an antibody to MPP6 followed by immunoblotting with an antibody to protein 4.1G. As shown in Fig. 2B, protein 4.1G was specifically detected after immunoprecipitation with the anti-MPP6 antibody. Similarly, MPP6 was specifically detected after immunoprecipitating 4.1G from sciatic nerves (Fig. 2B). In contrast, neither MPP6, nor 4.1G were detected when the immunoprecipitation was carried out using a control rabbit IgG. Thus, both directional IP studies indicate that MPP6 and 4.1G interact in myelinating Schwann cells. These immunoprecipitation studies were repeated three-times, and the blot lines were clearly detected anytime.

Analysis of the SLI in 4.1G$^{-/-}$ sciatic nerve.

To examine whether the reduced localization of MPP6 in the SLI reflects their abnormal formation, we compared the distribution of MPP6 with the known SLI protein E-cadherin (43), using confocal laser-scanning microscope (CLSM) (Fig. 3A). By accumulation of the Z-series optical sections (4.1G$^{+/+}$; Z-accum in Fig. 3A), the relationships among immunostained structures were recognized in wild type nerves: MPP6 was immunolocalized at SLIs, paranodes, abaxonal and mesoaxonal membranes together with E-cadherin. In

contrast, and in agreement with our IVCT-FS samples, the disappearance of MPP6 from the SLI was also noted by CLSM ($4.1G^{-/-}$; Z-accum, top lane in Fig. 3A). Some undefined cells other than the myelinated nerve fibers were also immunostained with anti-MPP6 Ab in both $4.1G^{+/+}$ and $4.1G^{-/-}$ sciatic nerves ($4.1G^{+/+}$ and $4.1G^{-/-}$; Z-accum, white arrows in Fig.3A). Although the MPP6 immunolocalization was not observed in SLI of $4.1G^{-/-}$ nerve fibers, E-cadherin was still detected ($4.1G^{-/-}$; Z-accum, middle lane in Fig. 3A). E-cadherin labeling also revealed that the shape of SLI in the $4.1G^{-/-}$ appeared different from that of wild type nerves. To further examine this point, we measured the circular truncated cone heights of the SLI (Fig. 3B). The E-cadherin positive-SLI height in the $4.1G^{-/-}$ mice was statistically lower than that in wild type animals (Fig. 3B).

Since E-cadherin labels adherens junctions that are present mostly at the outer edge of SLI (12, 43), we also used phalloidin to label filamentous actin that is present along the entire SLI structure (Fig. 3C). To evaluate necessity of the freeze-thaw treatment for the teased sciatic nerves, heights of the circular truncated cones were measured for both E-cadherin immunostaining and phalloidin staining with or without the freeze-thaw treatment (Figs. 3C and 3D). To obtain strong phalloidin staining, Triton X-100 treatment was useful (data not shown). An example of the double-fluorescence staining is demonstrated in Figure 3C. As previously reported (12, 43), E-cadherin immunoreactivity was restricted to the outer edge of the SLI either with, or without, the freeze-thaw treatment (Fig. 3C). In both cases, the heights

of the circular truncated cones of E-cadherin labeling were lower than those measured after phalloidin staining (Fig. 3D). Without the freeze-thaw treatment, heights of the circular truncated cones with the E-cadherin immunostaining were lower than those with the treatment (Fig. 3D), indicating usefulness of the freeze-thaw treatment for the E-cadherin immunostaining. As expected, for the phalloidin staining, the heights of the circular truncated cones without the freeze-thaw treatment were not different from those with the treatment (Fig. 3D). Accordingly, we measured the heights of the circular truncated cones in phalloidin-labeled nerves obtained from wild type and $4.1G^{-/-}$ nerve fibers without the frozen-thawed treatment (Fig. 3E). The heights in $4.1G^{-/-}$ nerve fibers were significantly lower than those of the wild type (Fig. 3F). These results suggest that protein 4.1G is required for the assembly of the SLI.

Immunolocalization of MPP6 in the seminiferous tubules of the $4.1G^{+/+}$ or $4.1G^{-/-}$ mice.

Previous studies revealed that MPP6 mRNA and protein are detected in testes (44). Therefore, we examined the distribution of MPP6 in the mouse seminiferous tubules by immunohistochemistry (Figs. 4A and 4B). MPP6 was mainly localized at basal parts of the seminiferous tubules, where it was detected along cell membranes in the spermatogonium and early spermatocytes (Fig. 4A- 4B). This immunostaining pattern of MPP6 was similar to that of 4.1G as we previously demonstrated (37).

We next determine whether the localization of MPP6 in the seminiferous tubules requires 4.1G. As depicted in Figure 4C, MPP6 was detected along cell membranes of the germ cells in both wild type and $4.1G^{-/-}$ mice. Given that protein 4.1B, another member of the 4.1 family is also found in the rodent seminiferous tubules (39), we examine the localization of MPP6 in mutant mice which lacks both protein 4.1B and 4.1G (Fig. 4D). MPP6 immunoreactivity was in germ cells was indistinguishable in 4.1B/G double mutant from wild type mice, indicating that in contrast to myelinating Schwann cells, the localization of MPP6 in the seminiferous tubules does not requires 4.1G.

DISCUSSION

In this study, we found that 4.1G interact with MPP6 and is required for the latter's targeting to cell membranes of the SLI in myelinating Schwann cells. In contrast, although MPP6 was detected in germ cells of mouse seminiferous tubules, especially in the spermatogonium and early spermatocytes, its localization in this tissue is independent on the presence of either 4.1G or 4.1B. This indicates that spermatogenic germ cells have a different mechanism for targeting of MPP6 to cell membranes compared to the Schwann cells.

MPP6 was originally identified in epithelial cells as a mammalian homologue of Lin-7 (mLin-7)-binding protein (15, 44), and is thought to play a role in targeting of proteins to basolateral surfaces. Although MPP6 was previously shown not to interact with 4.1R (44), we

demonstrate that it interact with 4.1G in myelinating Schwann cells. The existence of a MPP6-4.1G complex in mouse Schwann cells is analogous to the MPP1 (p55)-4.1R complex found in erythrocytes (22, 29, 33), CASK-4.1N interaction in neurons (3), and MPP6-4.1B interaction in epithelial cells (34). In the $4.1G^{-/-}$ mouse sciatic nerves, the total amount of MPP6 was significantly reduced, and the protein was abnormally detected in the cytoplasm near the Schwann cell nuclei. Nevertheless, MPP6 was still present at the paranodal loops even in the $4.1G^{-/-}$ sciatic nerves, indicating the independency of 4.1G in the MPP6 targeting to paranodes. MAGUK proteins are thought to function as scaffolding for cargoes and interact with motor molecules on microtubules (45). One of ezrin-radixin-moesin (ERM)-containing protein, merlin, was reported to directly interact with both microtubules (48) and kinesin motor proteins (2). Although merlin was also reported to be expressed in Schwann cells (32), our results indicate that it is not related to the MPP6 targeting to SLIs. However, a temporal and spatial study for such ERM protein, merlin, and 4.1G-MPP6 on microtubules will be a further interesting study.

It is interesting that the size of SLIs in the aged $4.1G^{-/-}$ mice was different from that in wild type mice, as revealed by both E-cadherin and actin staining. A MAGUKs, MPP5 (Pals1), was reported to regulate the E-cadherin trafficking in mammalian epithelial cells (47). On the other hand, another 4.1 family protein, 4.1R, was shown to link to E-cadherin/β-catenin in mouse stomach epithelial cells (50). We believe that the MPP6-4.1G

complex affects to maintenance of the SLI structure during aging. It is well known that 4.1R-deficient erythrocytes become elliptocytes from normal biconcave discs depending on the age of the erythrocytes, due to gradual instability of functional membrane skeletons to resist mechanical strength under circulation (19). As the length of PNS nerve fibers easily change with mechanical stretching in animal bodies during exercise, it is possible that the SLI present along myelin internodes in the PNS may have a role in protecting peripheral nerves during mechanical external forces. For the specific membrane-adhesion structure in internodes, SLI have various tight and adherens junctional molecules (28), such as claudin (28)), occludin (1), E-cadherin (43, 51), and junctional adhesion molecule (JAM)-C (31). In this paper, we demonstrated that the MPP6-4.1G complex has a functional role the long-term maintenance of the SLI structures. Because spectrin-actin (35) and MPP6-4.1G are localized in SLIs, more precise ultrastructural study will be needed to reveal functional mechanism of the membrane skeletons at this location.

A further question is what would happen if MPP6 is deficient for 4.1G targeting as well as for SLI formation? Requirement of MPP6 was reported for the maturation and function of *Drosophila* septate junctions (20). In addition, other MAGUKs, such as Dlg1 (5, 6, 8, 13) and MPP5 (25) were reported to affect myelination if they were deficient due to disruption of the phosphatidylinositol metabolism with Mtmr (myotubularin-related)-2 and PTEN (phosphatase and tensin homolog). On the other hand, it has been demonstrated that MAGUK

families interact with each other, such as Dlg1 and MPP7 in epithelial cells (4). Therefore, examination of the relationships between MPP6, MPP5 in Schwann cells will be needed.

In addition, the dependence of MPP6 on formation of mammalian seminiferous tubules is another concern because Dlg was reported to function in gamete development in *Drosophila* testes (26). Compared to the Schwann cells, it is interesting that disappearance of the MPP6 targeting was not detected in the testicular germ cells in $4.1G^{-/-}$ and $4.1B^{-/-}$ mice, as shown in Figures 4C and 4D. It is important to examine the mechanism of the 4.1G targeting of MPP6 to solve the question why such different events happened in different organs.

ACKNOWLEDGMENT

This work was partially supported by a grant from the Japanese Society for the Promotion of Science (KAKEN #21590214) to N. Terada, and the National Institutes of Health (NS50220) to E. Peles. The authors thank Mr. Yutaka Kitahara in Department of Anatomy and Molecular Histology, Interdisciplinary Graduate School of Medicine and Engineering, University of Yamanashi, for his technical assistance.

References

1. **Alanne, M. H., K. Pummi, A. M. Heape, R. Grenman, J. Peltonen, and S. Peltonen.** 2009. Tight junction proteins in human Schwann cell autotypic junctions. J Histochem Cytochem **57:**523-529.
2. **Bensenor, L. B., K. Barlan, S. E. Rice, R. G. Fehon, and V. I. Gelfand.** 2010. Microtubule-mediated transport of the tumor-suppressor protein Merlin and its mutants. Proc Natl Acad Sci U S A **107:**7311-7316.
3. **Biederer, T., and T. C. Sudhof.** 2001. CASK and protein 4.1 support F-actin nucleation on neurexins. J Biol Chem **276:**47869-47876.
4. **Bohl, J., N. Brimer, C. Lyons, and S. B. Vande Pol.** 2007. The stardust family protein MPP7 forms a tripartite complex with LIN7 and DLG1 that regulates the stability and localization of DLG1 to cell junctions. J Biol Chem **282:**9392-9400.
5. **Bolino, A., A. Bolis, S. C. Previtali, G. Dina, S. Bussini, G. Dati, S. Amadio, U. Del Carro, D. D. Mruk, M. L. Feltri, C. Y. Cheng, A. Quattrini, and L. Wrabetz.** 2004. Disruption of Mtmr2 produces CMT4B1-like neuropathy with myelin outfolding and impaired spermatogenesis. J Cell Biol **167:**711-721.
6. **Bolis, A., S. Coviello, I. Visigalli, C. Taveggia, A. Bachi, A. H. Chishti, T. Hanada, A. Quattrini, S. C. Previtali, A. Biffi, and A. Bolino.** 2009. Dlg1, Sec8, and Mtmr2 regulate membrane homeostasis in Schwann cell myelination. J Neurosci **29:**8858-8870.
7. **Chen, J., N. Terada, N. Ohno, S. Saitoh, Y. Saitoh, and S. Ohno.** 2011. Immunolocalization of membrane skeletal protein, 4.1G, in enteric glial cells in the mouse large intestine. Neurosci Lett **488:**193-198.
8. **Cotter, L., M. Ozcelik, C. Jacob, J. A. Pereira, V. Locher, R. Baumann, J. B. Relvas, U. Suter, and N. Tricaud.** 2010. Dlg1-PTEN interaction regulates myelin thickness to prevent damaging peripheral nerve overmyelination. Science **328:**1415-1418.
9. **de Mendoza, A., H. Suga, and I. Ruiz-Trillo.** 2010. Evolution of the MAGUK protein gene family in premetazoan lineages. BMC Evol Biol **10:**93.
10. **Discher, D. E., R. Winardi, P. O. Schischmanoff, M. Parra, J. G. Conboy, and N. Mohandas.** 1995. Mechanochemistry of protein 4.1's spectrin-actin-binding domain: ternary complex interactions, membrane binding, network integration, structural strengthening. J Cell Biol **130:**897-907.
11. **Funke, L., S. Dakoji, and D. S. Bredt.** 2005. Membrane-associated guanylate kinases regulate adhesion and plasticity at cell junctions. Annu Rev Biochem **74:**219-245.
12. **Ghabriel, M. N., and G. Allt.** 1981. Incisures of Schmidt-Lanterman. Progress in neurobiology **17:**25-58.
13. **Goebbels, S., J. H. Oltrogge, R. Kemper, I. Heilmann, I. Bormuth, S. Wolfer, S. P. Wichert, W. Mobius, X. Liu, C. Lappe-Siefke, M. J. Rossner, M. Groszer, U. Suter, J. Frahm, S.**

Boretius, and K. A. Nave. 2010. Elevated phosphatidylinositol 3,4,5-trisphosphate in glia triggers cell-autonomous membrane wrapping and myelination. J Neurosci **30:**8953-8964.

14. **Hanada, T., A. Takeuchi, G. Sondarva, and A. H. Chishti.** 2003. Protein 4.1-mediated membrane targeting of human discs large in epithelial cells. J Biol Chem **278:**34445-34450.
15. **Kamberov, E., O. Makarova, M. Roh, A. Liu, D. Karnak, S. Straight, and B. Margolis.** 2000. Molecular cloning and characterization of Pals, proteins associated with mLin-7. J Biol Chem **275:**11425-11431.
16. **Lozovatsky, L., N. Abayasekara, S. Piawah, and Z. Walther.** 2009. CASK deletion in intestinal epithelia causes mislocalization of LIN7C and the DLG1/Scrib polarity complex without affecting cell polarity. Mol Biol Cell **20:**4489-4499.
17. **Lue, R. A., E. Brandin, E. P. Chan, and D. Branton.** 1996. Two independent domains of hDlg are sufficient for subcellular targeting: the PDZ1-2 conformational unit and an alternatively spliced domain. J Cell Biol **135:**1125-1137.
18. **Lue, R. A., S. M. Marfatia, D. Branton, and A. H. Chishti.** 1994. Cloning and characterization of hdlg: the human homologue of the Drosophila discs large tumor suppressor binds to protein 4.1. Proc Natl Acad Sci U S A **91:**9818-9822.
19. **Mohandas, N., and P. G. Gallagher.** 2008. Red cell membrane: past, present, and future. Blood **112:**3939-3948.
20. **Moyer, K. E., and J. R. Jacobs.** 2008. Varicose: a MAGUK required for the maturation and function of Drosophila septate junctions. BMC Dev Biol **8:**99.
21. **Nix, S. L., A. H. Chishti, J. M. Anderson, and Z. Walther.** 2000. hCASK and hDlg associate in epithelia, and their src homology 3 and guanylate kinase domains participate in both intramolecular and intermolecular interactions. J Biol Chem **275:**41192-41200.
22. **Nunomura, W., Y. Takakuwa, M. Parra, J. Conboy, and N. Mohandas.** 2000. Regulation of protein 4.1R, p55, and glycophorin C ternary complex in human erythrocyte membrane. J Biol Chem **275:**24540-24546.
23. **Ohno, N., N. Terada, M. Komada, S. Saitoh, F. Costantini, V. Pace, P. G. Germann, K. Weber, H. Yamakawa, O. Ohara, and S. Ohno.** 2009. Dispensable role of protein 4.1B/DAL-1 in rodent adrenal medulla regarding generation of pheochromocytoma and plasmalemmal localization of TSLC1. Biochim Biophys Acta **1793:**506-515.
24. **Ohno, N., N. Terada, H. Yamakawa, M. Komada, O. Ohara, B. D. Trapp, and S. Ohno.** 2006. Expression of protein 4.1G in Schwann cells of the peripheral nervous system. J Neurosci Res **84:**568-577.
25. **Ozcelik, M., L. Cotter, C. Jacob, J. A. Pereira, J. B. Relvas, U. Suter, and N. Tricaud.** 2010. Pals1 is a major regulator of the epithelial-like polarization and the extension of the myelin sheath in peripheral nerves. J Neurosci **30:**4120-4131.
26. **Papagiannouli, F., and B. M. Mechler.** 2009. discs large regulates somatic cyst cell survival

and expansion in Drosophila testis. Cell Res **19:**1139-1149.

27. **Parra, M., P. Gascard, L. D. Walensky, S. H. Snyder, N. Mohandas, and J. G. Conboy.** 1998. Cloning and characterization of 4.1G (EPB41L2), a new member of the skeletal protein 4.1 (EPB41) gene family. Genomics **49:**298-306.
28. **Poliak, S., S. Matlis, C. Ullmer, S. S. Scherer, and E. Peles.** 2002. Distinct claudins and associated PDZ proteins form different autotypic tight junctions in myelinating Schwann cells. J Cell Biol **159:**361-372.
29. **Quinn, B. J., E. J. Welch, A. C. Kim, M. A. Lokuta, A. Huttenlocher, A. A. Khan, S. M. Kuchay, and A. H. Chishti.** 2009. Erythrocyte scaffolding protein p55/MPP1 functions as an essential regulator of neutrophil polarity. Proc Natl Acad Sci U S A **106:**19842-19847.
30. **Saitoh, Y., N. Terada, S. Saitoh, N. Ohno, Y. Fujii, and S. Ohno.** 2010. Histochemical approach of cryobiopsy for glycogen distribution in living mouse livers under fasting and local circulation loss conditions. Histochem Cell Biol **133:**229-239.
31. **Scheiermann, C., P. Meda, M. Aurrand-Lions, R. Madani, Y. Yiangou, P. Coffey, T. E. Salt, D. Ducrest-Gay, D. Caille, O. Howell, R. Reynolds, A. Lobrinus, R. H. Adams, A. S. Yu, P. Anand, B. A. Imhof, and S. Nourshargh.** 2007. Expression and function of junctional adhesion molecule-C in myelinated peripheral nerves. Science **318:**1472-1475.
32. **Scherer, S. S., and D. H. Gutmann.** 1996. Expression of the neurofibromatosis 2 tumor suppressor gene product, merlin, in Schwann cells. J Neurosci Res **46:**595-605.
33. **Seo, P. S., J. J. Jeong, L. Zeng, C. G. Takoudis, B. J. Quinn, A. A. Khan, T. Hanada, and A. H. Chishti.** 2009. Alternatively spliced exon 5 of the FERM domain of protein 4.1R encodes a novel binding site for erythrocyte p55 and is critical for membrane targeting in epithelial cells. Biochim Biophys Acta **1793:**281-289.
34. **Shingai, T., W. Ikeda, S. Kakunaga, K. Morimoto, K. Takekuni, S. Itoh, K. Satoh, M. Takeuchi, T. Imai, M. Monden, and Y. Takai.** 2003. Implications of nectin-like molecule-2/IGSF4/RA175/SgIGSF/TSLC1/SynCAM1 in cell-cell adhesion and transmembrane protein localization in epithelial cells. J Biol Chem **278:**35421-35427.
35. **Susuki, K., A. R. Raphael, Y. Ogawa, M. C. Stankewich, E. Peles, W. S. Talbot, and M. N. Rasband.** 2011. Schwann cell spectrins modulate peripheral nerve myelination. Proc Natl Acad Sci U S A **108:**8009-8014.
36. **Terada, N., N. Ohno, S. Saitoh, Y. Saitoh, Y. Fujii, T. Kondo, R. Katoh, C. Chan, S. N. Abraham, and S. Ohno.** 2009. Involvement of dynamin-2 in formation of discoid vesicles in urinary bladder umbrella cells. Cell Tissue Res **337:**91-102.
37. **Terada, N., N. Ohno, S. Saitoh, Y. Saitoh, M. Komada, H. Kubota, and S. Ohno.** 2010. Involvement of a membrane skeletal protein, 4.1G, for Sertoli/germ cell interaction. Reproduction **139:**883-892.
38. **Terada, N., N. Ohno, S. Saitoh, Y. Saitoh, and S. Ohno.** 2009. Immunoreactivity of glutamate in mouse retina inner segment of photoreceptors with in vivo cryotechnique. J

Histochem Cytochem **57:**883-888.

39. **Terada, N., N. Ohno, H. Yamakawa, T. Baba, Y. Fujii, Z. Zea, O. Ohara, and S. Ohno.** 2004. Immunohistochemical study of protein 4.1B in the normal and W/W(v) mouse seminiferous epithelium. J Histochem Cytochem **52:**769-777.
40. **Terada, N., N. Ohno, H. Yamakawa, O. Ohara, X. Liao, T. Baba, and S. Ohno.** 2005. Immunohistochemical study of a membrane skeletal molecule, protein 4.1G, in mouse seminiferous tubules. Histochem Cell Biol **124:**303-311.
41. **Terada, N., Y. Saitoh, S. Saitoh, N. Ohno, T. Jin, and S. Ohno.** 2010. Visualization of microvascular blood flow in mouse kidney and spleen by quantum dot injection with "in vivo cryotechnique". Microvasc Res **80:**491-498.
42. **Trapp, B. D., S. B. Andrews, A. Wong, M. O'Connell, and J. W. Griffin.** 1989. Co-localization of the myelin-associated glycoprotein and the microfilament components, F-actin and spectrin, in Schwann cells of myelinated nerve fibres. J Neurocytol **18:**47-60.
43. **Tricaud, N., C. Perrin-Tricaud, J. L. Bruses, and U. Rutishauser.** 2005. Adherens junctions in myelinating Schwann cells stabilize Schmidt-Lanterman incisures via recruitment of p120 catenin to E-cadherin. J Neurosci **25:**3259-3269.
44. **Tseng, T. C., S. M. Marfatia, P. J. Bryant, S. Pack, Z. Zhuang, J. E. O'Brien, L. Lin, T. Hanada, and A. H. Chishti.** 2001. VAM-1: a new member of the MAGUK family binds to human Veli-1 through a conserved domain. Biochim Biophys Acta **1518:**249-259.
45. **Verhey, K. J., and T. A. Rapoport.** 2001. Kinesin carries the signal. Trends Biochem Sci **26:**545-550.
46. **Walensky, L. D., P. Gascard, M. E. Fields, S. Blackshaw, J. G. Conboy, N. Mohandas, and S. H. Snyder.** 1998. The 13-kD FK506 binding protein, FKBP13, interacts with a novel homologue of the erythrocyte membrane cytoskeletal protein 4.1. J Cell Biol **141:**143-153.
47. **Wang, Q., X. W. Chen, and B. Margolis.** 2007. PALS1 regulates E-cadherin trafficking in mammalian epithelial cells. Mol Biol Cell **18:**874-885.
48. **Xu, H. M., and D. H. Gutmann.** 1998. Merlin differentially associates with the microtubule and actin cytoskeleton. J Neurosci Res **51:**403-415.
49. **Yamada, K. H., T. Hanada, and A. H. Chishti.** 2007. The effector domain of human Dlg tumor suppressor acts as a switch that relieves autoinhibition of kinesin-3 motor GAKIN/KIF13B. Biochemistry **46:**10039-10045.
50. **Yang, S., X. Guo, G. Debnath, N. Mohandas, and X. An.** 2009. Protein 4.1R links E-cadherin/beta-catenin complex to the cytoskeleton through its direct interaction with beta-catenin and modulates adherens junction integrity. Biochim Biophys Acta **1788:**1458-1465.
51. **Young, P., O. Boussadia, P. Berger, D. P. Leone, P. Charnay, R. Kemler, and U. Suter.** 2002. E-cadherin is required for the correct formation of autotypic adherens junctions of the outer mesaxon but not for the integrity of myelinated fibers of peripheral nerves. Mol Cell

Neurosci **21:**341-351.

FIGURE LEGENDS

FIG. 1. Immunolocalization of MPP6 in the $4.1G^{+/+}$ (A) and $4.1G^{-/-}$ (B) mouse sciatic nerves with "in vivo cryotechnique". Right lanes in A and B show differential interference contrast (DIC) images to demonstrate each nerve fiber. Although the MPP6 immunolocalization is obvious in SLIs of the $4.1G^{+/+}$ nerves (arrows in A), it is only detected around the nuclei in the $4.1G^{-/-}$ nerves (arrowheads in B). White arrow shows the MPP6 immunolocalization in paranodes beside the node of Ranvier. (C) Immunoblotting for MPP6 lysates of sciatic nerves in the $4.1G^{+/+}$ (lanes 1, 2) or $4.1G^{-/-}$ (lanes 3, 4) mouse sciatic nerves. Two different mouse samples from each group are shown as examples. The intensity of the 55-kD line (arrows) in the $4.1G^{-/-}$ mice was markedly reduced compared to that in the $4.1G^{+/+}$ mice. Arrowheads indicates weaker blotted line (less than 30-kD) probably due to an isoform or non-specific reaction. MM: molecular marker. Bars, 10 μm.

FIG. 2. Immunolocalization of MPP6 and 4.1G in serial sections of mouse sciatic nerves with "in vivo cryotechnique" (A) and immunoprecipitation (IP) study of the MPP6-4.1G interaction (B and C). (A) Arrows with S1-S6 labels indicate corresponding SLIs with the MPP6 (top) and 4.1G (bottom) immunostaining, and their immunolocalization in SLIs is largely matching. (B and C) Lanes 1 shows the 4.1G (Fig. 2B) or MPP6 (Fig. 2C) immunoblotting of the intact sciatic nerve lysates. Lanes 2-7 show the 4.1G (Fig. 2B) or

MPP6 (Fig. 2C) immunoblotting for three different samples as follows. Sciatic nerve lysates are included in the samples of lanes 2, 3, 5 and 6, but not in that of lane 4 and 7 (Figs. 2B and 2C); confirming that original mouse IgG was completely depleted by the Sepharose-G pre-treatment. The MPP6 (Fig. 2B) or 4.1G (Fig.2C) Ab is included in samples of lanes 2 and 4 for IP, but not in that of lane 3; indicating that the 50-kD line is derived from the anti-MPP6 (Fig. 2B) or anti-4.1G (Fig. 2C) antibody-derived IgG proteins (arrowheads in Fig. 2B and 2C; IgG). Arrows in Figs. 2B and 2C indicate the molecular weights of 4.1G (around 110-kD in Fig. 2B) and MPP6 (around 55-kD in Fig. 2C), respectively, and the lines at the same molecular weights in lane 2, but not in lanes 3 and 4 (Fig. 2B and 2C); indicating interaction of the proteins. Rabbit IgG (rIgG) is included in samples of lanes 5 and 7, but no 110-kD (Fig. 2B) or 55-kD (Fig. 2C) line appeared; indicating no reaction of rIgG to 4.1G or MPP6. Bar, 20 μm (A).

FIG. 3. MPP6 and E-cadherin (E-cad) immunolocalization and phalloidin staining in $4.1G^{+/+}$ and $4.1G^{-/-}$ mouse-teased sciatic nerves. (A: $4.1G^{+/+}$; S15) Confocal laser scanning micrographs (CLSMs) of MPP6 (green) and E-cad (red) immunostaining of the 15th optical section. Micrographs in the bottom lane show merged images of the two immunostainings, indicating colocalization of 4.1G and E-cad in mesoaxons (arrowheads) and SLIs (arrows). Insets show highly magnified views of parts of the SLIs. (A: $4.1G^{+/+}$ and $4.1G^{-/-}$; Z-accum)

Accumulated Z-series from 70 optical sections (0.5 μm each) of the MPP6 (green), E-cad (red), and merged images in the $4.1G^{+/+}$ and $4.1G^{-/-}$ sciatic nerves. Insets show highly magnified view of a part of SLIs. Note the disappearance of the MPP6 immunostaining in SLIs of the $4.1G^{-/-}$ sciatic nerves (arrows in $4.1G^{-/-}$). Some cells other than myelinated nerve fibers are immunostained with the anti-MPP6 antibody (white arrowheads in $4.1G^{+/+}$). (B) Statistic analysis for the heights of the circular truncated cones of SLIs (n=600) in sciatic nerves of three aged (10-months-old) $4.1G^{+/+}$ and $4.1G^{-/-}$ mice. The heights of the circular truncated cones of SLIs in the $4.1G^{-/-}$ are lower than those in the $4.1G^{+/+}$ ones. **P<0.01. (C) Example of a CLSM of the double staining for E-cad (red) and filamentous actin (Phalloidin; green), and their merged image (Merged) in the teased sciatic nerves with the frozen-thawed treatment. Although both E-cad and phalloidin staining colocalize at the outside edge of SLIs (arrows), phalloidin staining is detected alone near the inner edge (arrowheads). (D) Statistic analysis for heights of the circular truncated cones of SLIs (n=300) in teased sciatic nerves with Triton X-100 treatment alone (Triton) or freeze-thaw treatment before the Triton treatment (Freeze-thaw + Triton). *P<0.05, **P<0.01. (E) Representative CLSM of teased sciatic nerves with phalloidin staining in $4.1G^{+/+}$ or $4.1G^{-/-}$ mice. Structure of the circular truncated cones of SLIs in the $4.1G^{-/-}$ nerve fibers (arrowheads) is different from that in $4.1G^{+/+}$ ones (arrows). (F) Statistic analysis for heights of the circular truncated cones of SLIs (n=600) in teased sciatic nerves in three $4.1G^{+/+}$ or $4.1G^{-/-}$ mice. Bars, 10 μm.

FIG. 4. Immunostaining of MPP6 in seminiferous tubules for perfusion fixation followed by sucrose embedding for the $4.1G^{+/+}B^{+/+}$ (A, B), $4.1G^{-/-}B^{+/+}$ (C), and $4.1G^{-/-}B^{-/-}$ (D) mice. (A) With light microscopic images, MPP6 is immunolocalized in germ cells in the basal parts of the seminiferous tubules at stages V (left lane) and X (right lane), indicating the spermatogonium and early spermatocytes. Intensity of the MPP6 immunostaining in the arch-shape spermatogonium is obvious at stage X (arrowheads). (B) With immunoelectron microscopy, DAB-reaction products with the anti-MPP6 antibody are detected (arrows) under cell membranes of spermatocytes (Sc). Se; Sertoli cell process. The bottom image shows a higher magnified view of the rectangle part of the upper image. (C and D) In the $4.1G^{-/-}B^{+/+}$ (C), and $4.1G^{-/-}B^{-/-}$ (D) mice, MPP6 immunostaining was detected in the basal parts of the seminiferous tubules (arrowheads). Bars, 20 μm (A, C, D); 1 μm (B).

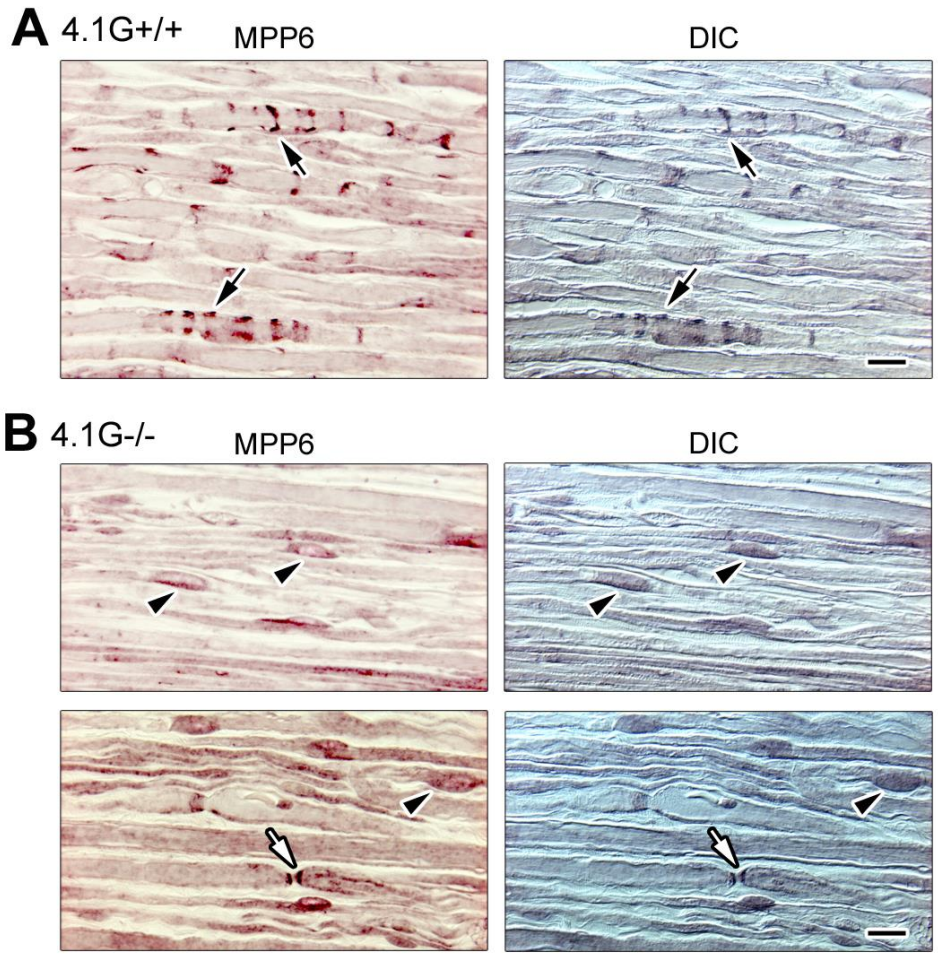
A 4.1G+/+
MPP6
DIC
B 4.1G-/-
MPP6
DIC

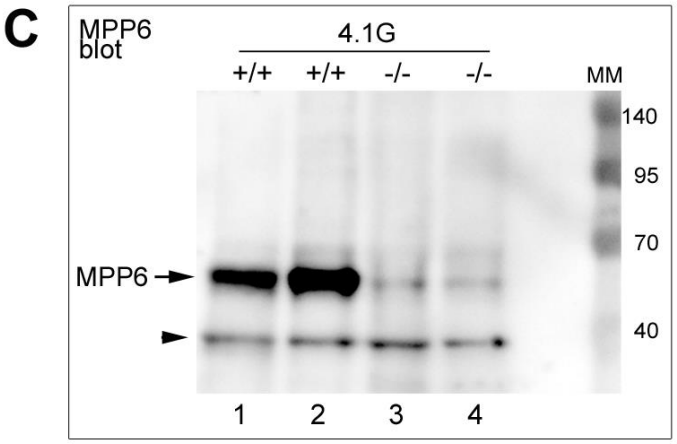
C
MPP6 blot
4.1G
+/+
+/+
-/-
-/-
MM
140
95
70
40
MPP6
1
2
3
4

Fig.1

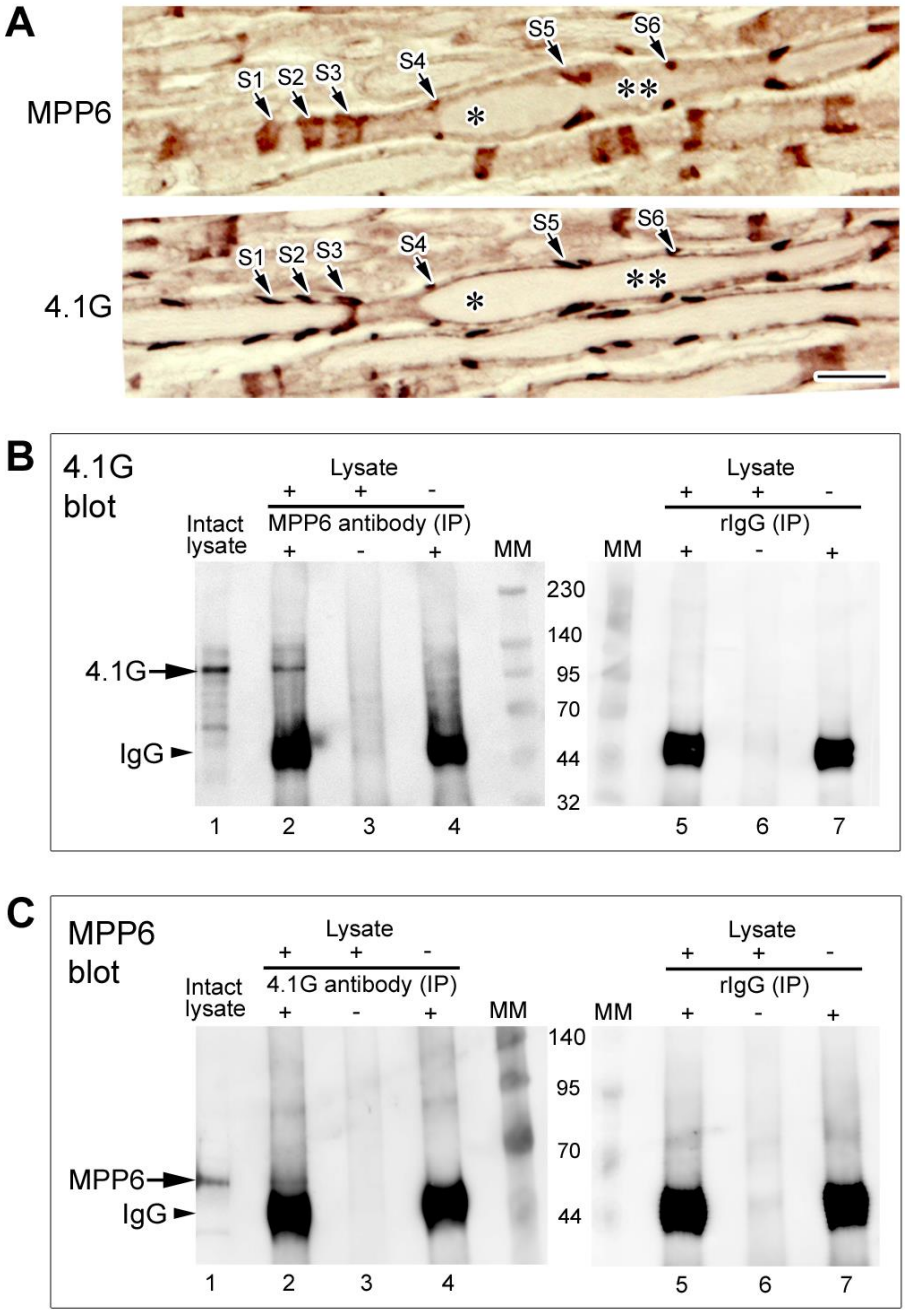
A
MPP6
4.1G
S1
S2
S3
S4
S5
S6
*
**
B
4.1G blot
Lysate
Intact lysate
MPP6 antibody (IP)
rIgG (IP)
MM
4.1G
IgG
230
140
95
70
44
32
1
2
3
4
5
6
7
C
MPP6 blot
4.1G antibody (IP)
MPP6
IgG
140
95
70
44

Fig.2

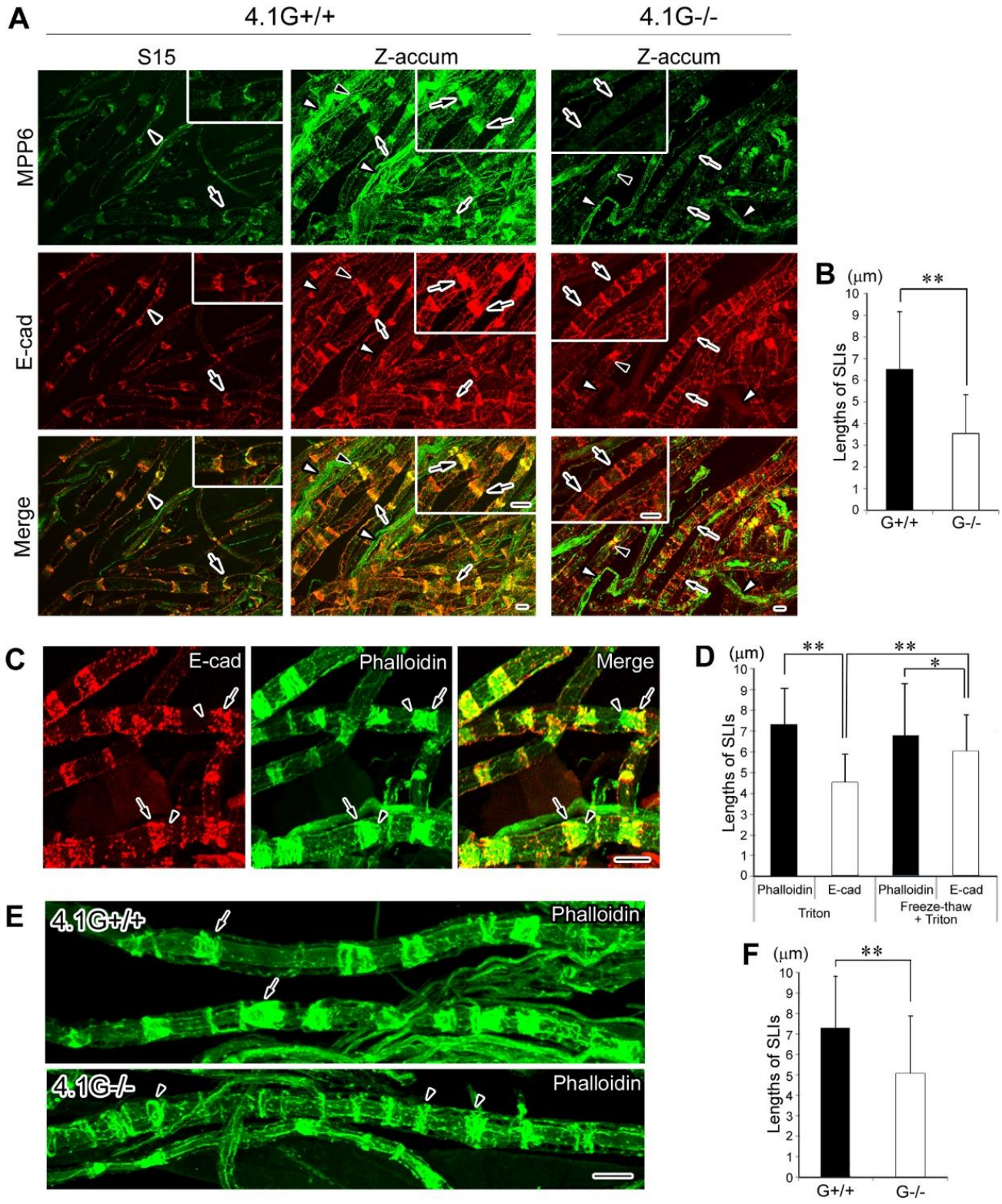
A
4.1G+/+
4.1G-/-
S15
Z-accum
Z-accum
MPP6
E-cad
Merge
B
(μm)
**
Lengths of SLIs
G+/+
G-/-
C
E-cad
Phalloidin
Merge
D
(μm)
**
**
*
Lengths of SLIs
Phalloidin
E-cad
Phalloidin
E-cad
Triton
Freeze-thaw
+ Triton
E
4.1G+/+
Phalloidin
4.1G-/-
Phalloidin
F
(μm)
**
Lengths of SLIs
G+/+
G-/-

Fig.3

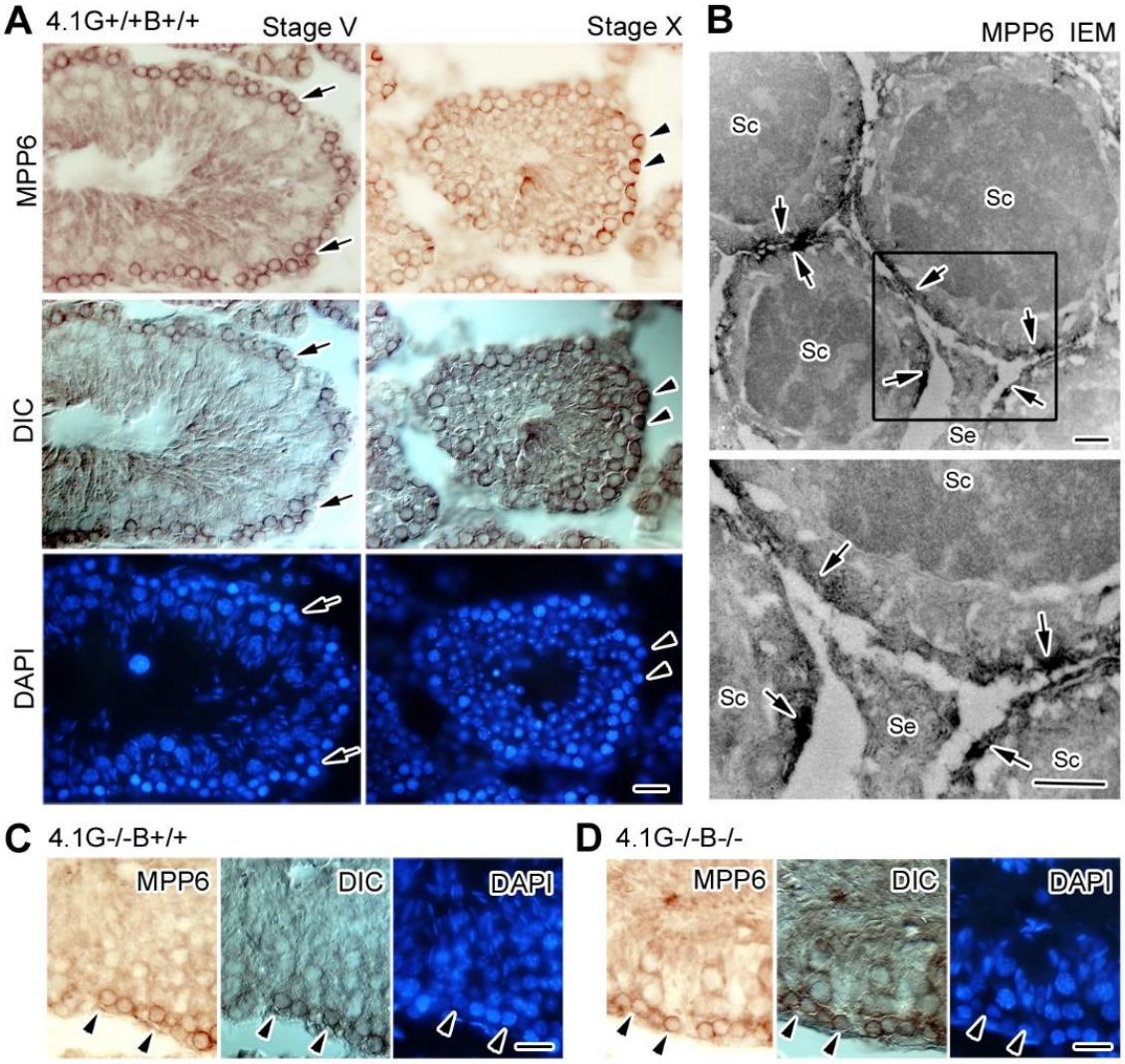
A
4.1G+/+B+/+
Stage V
Stage X
MPP6
DIC
DAPI
B
MPP6 IEM
Sc
Sc
Sc
Se
Sc
Sc
Se
Sc
C
4.1G-/-B+/+
MPP6
DIC
DAPI
D
4.1G-/-B-/-
MPP6
DIC
DAPI

Fig.4